Transactions of the Korean Nuclear Society Spring Meeting

Jeju, Korea, May 22-23, 2025

Modeling Heat Transfer in Helically Coiled Steam Generators Using Different Correlations

Hyochan Kim, Jun Ha Hwang, Jeong Ik Lee

Department of Nuclear and Quantum Engineering, Korea Advanced Institute of Science and Technology, 373-1 Guseong-dong Yuseong-gu, Daejeon 305-701, Republic of Korea

** Corresponding author: jeongiklee@kaist.ac.kr*

Keywords: high-temperature gas reactor, helium, helical steam generator, heat transfer, modeling

1. Introduction

Small Modular Reactors (SMRs) have been recognized as a promising clean energy source that could solve climate change. Helical steam generators (HSGs) have become the preferred option as their surface-area-to-volume ratio is large.

In recent studies, engineers have carried out both numerical and laboratory experiments to test the heat transfer phenomena of HSGs. These studies provide insights into pressure and temperature fluctuations inside the tubes carrying pressurized fluids. Geometric parameters vary among SMRs depending on their operating conditions.

This study aims to find optimal correlations in developing a computational model of heat transfer between the primary and secondary coolants of HTR-PM, an SMR that utilizes high-temperature Helium as the primary coolant. Most fluid parameters are disclosed to the public, and undisclosed ones are gathered from other research and approximated based on the parameters of HTR-10 [1], the predecessor model of HTR-PM.

2. Methodology

This section discusses design and operating parameters. The correlations incorporated into the model are also outlined.

2.1 HSG design and operating parameters

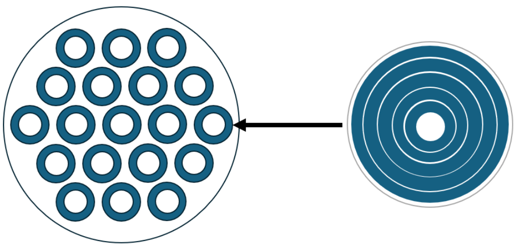

Figure 1: Cross-section of HTR-PM steam generator's shell side and tube side

HTR-PM is composed of two 250 MW_{th} reactors. Helium is heated inside each reactor and subsequently sent to the respective HSGs. Each HSG consists of 19 individual steam generators, and each steam generator is split into 5 layers of 5, 6, 7, 8, and 9 tubes, respectively, as shown in Fig. 1; A total of 665 tubes carry feedwater that is heated to steam [2]. This study assumes that the flow of water and heat transfer behavior is homogeneous. Thus, the system can be represented as a single tube and shell system, where a single tube is averaged from all tubes.

Table I: Geometric parameters of HTR-PM's steam generator

Parameter	Primary	Secondary
Inlet Temperature [°C]	750	205
Outlet Temperature [°C]	250	566
Inlet Pressure [MPa]	7.0	13.24
Mass Flow Rate [kg/s]	96	95 *
Shell Height [m]	8.6	
Average Helical Diameter, D_c [m]	0.215 *	
Tube Inner / Outer Diameter, d_i / d_o [mm]	17 / 19	
Tube Vertical / Horizontal Pitch [mm]	30 / 25	
Tube Thermal Conductivity [W/m K]	T22: 32.1~37.2 (205~643°C) Incoloy 800H: 22.2 (643°C~)	

* Assumed values

In Table I, the geometric parameters that were used in the code are listed. The tube is composed of two different materials: T22 is used for regions below 643°C and Incoloy 800H is used for regions above 643°C [3].

2.2 Heat Transfer Correlations

Table II and III list correlations that were used in the numerical model for HTR-PM [2]. Since Helium does not undergo a phase change, only one correlation is used for heat transfer and pressure drop. Water undergoes a phase change from liquid to vapor, so multiple correlations are required to model the heat transfer behavior across different flow zones.

Table II: Correlations for calculating heat transfer coefficient at different zones of fluid flow

Zone	Correlations	Researchers
Single-phase liquid zone (shell side)	$Nu_{He} = \begin{cases} 0.9Re_{He}^{0.4}Pr_{He}^{0.36}\left(\frac{Pr_{He}}{Pr_{wall}}\right)^{0.25}, Re_{He} < 100 \\ 0.52Re_{He}^{0.5}Pr_{He}^{0.36}\left(\frac{Pr_{He}}{Pr_{wall}}\right)^{0.25}, Re_{He} < 1{,}000 \\ 0.27Re_{He}^{0.63}Pr_{He}^{0.36}\left(\frac{Pr_{He}}{Pr_{wall}}\right)^{0.25}, Re_{He} < 200{,}000 \\ 0.033Re_{He}^{0.8}Pr_{He}^{0.4}\left(\frac{Pr_{He}}{Pr_{wall}}\right)^{0.25}, Re_{He} > 200{,}000 \end{cases}$	Žukauskas
Single-phase liquid zone (tube side)	$Nu = \begin{cases} 3.65 + 0.08[1 + 0.08\left[1 + 0.8\left(\frac{d_i}{D_c}\right)^{0.9} Re^a Pr^{\frac{1}{3}}\right], \\ Re < Re_{cr} \\ 0.023\left[1 + 14.8\left(1 + \frac{d_i}{D_c}\right)\left(\frac{d_i}{D_c}\right)^{1.3}\right] Re^b Pr^{\frac{1}{3}}, \\ Re_{cr} < Re < 22{,}000 \\ 0.023\left[1 + 3.6\left(1 - \frac{d_i}{D_c}\right)\left(\frac{d_i}{D_c}\right)^{0.8}\right] Re^{0.8} Pr^{\frac{1}{3}}, \\ 22{,}000 < Re < 150{,}000 \end{cases}$ $a = 0.5 + 0.2903\left(\frac{d_i}{D_c}\right)^{0.194}$ $b = 0.8 - 0.22\left(\frac{d_i}{D_c}\right)^{0.1}$	Schmidt
Subcooled boiling zone	$Nu = 0.0456\left(\frac{d_i}{D_c}\right)^{0.16} Re^{0.8}Pr^{0.4}$	Hardik
Saturated boiling and forced convection evaporation zone	$h = Fh_l + Sh_{nb},$ $h_l = 0.023Re_l^{0.8}Pr_l^{0.4}\left(\frac{k_l}{d_i}\right) \times \left(Re_l\left(\frac{d_i}{D_c}\right)^2\right)^{1/20}$ $h_{nb} = 0.00122\left(\frac{k_l^{0.79}c_{p,l}^{0.45}\rho_l^{0.49}}{\sigma^{0.5}h_{fg}^{0.24}\rho_g^{0.24}\mu_l^{0.29}}\right)\Delta T_{sat}^{0.24}\Delta P_{sat}^{0.75}$ $F = \begin{cases} 1.0, X_{tt}^{-1} \le 0.1 \\ F = min\begin{cases} 2.35\left(\frac{1}{X_{tt}} + 0.213\right)^{0.736} \\ 70.0 \end{cases}, X_{tt}^{-1} > 0.1' \end{cases}$ $X_{tt}^{-1} = \left(\frac{x}{1-x}\right)^{0.9}\left(\frac{\rho_l}{\rho_g}\right)^{0.5}\left(\frac{\mu_g}{\mu_l}\right)^{0.1}$ $S = \begin{cases} \frac{1}{[1 + 0.12Re_{TP}]^{1.14}}, Re_{TP} < 32.5 \\ \frac{1}{[1 + 0.42(Re_{TP})^{0.78}]}, 32.5 \le Re_{TP} < 70.0' \\ 0.0797, Re_{TP} \ge 70 \end{cases}$ $Re_{TP} = \left[\frac{G_m(1-x)d_i}{\mu_l}\right] F^{1.25} \times 10^{-4}$	Yang's revision of Chen
Liquid deficiency zone	$Nu = 0.023YRe^{0.85}\left[x + \frac{\rho_g}{\rho_l}(1-x)\right]^{0.80} Pr_{wall}^{0.8},$ $Y = 1 - 0.1\left(\frac{\rho_l}{\rho_g} - 1\right)^{0.4}(1-x)^{0.4}$	Xu and Jia's revision of Miropol'skiy
Single-phase vapor zone	$h = \begin{cases} 0.02439\frac{k}{d}Re^{0.8333}Pr^{0.4}\left(\frac{d_i}{D_c}\right)^{\frac{1}{12}}\left[1 + \frac{0.061}{\left[Re\left(\frac{d_i}{D_c}\right)^{2.5}\right]^{\frac{1}{6}}}\right], Pr > 1 \\ 0.03846\frac{k}{d}Re^{0.8}\frac{Pr}{Pr^{\frac{2}{3}} - 0.074}\left(\frac{d_i}{D_c}\right)^{\frac{1}{10}}\left[1 + \frac{0.098}{\left[Re\left(\frac{d_i}{D_c}\right)^2\right]^{\frac{1}{5}}}\right], Pr < 1 \end{cases}$	Mori & Nakayama

Table III: Correlations for calculating the pressure drop of fluid flow

Zone	Correlations	Researchers
Single-phase liquid zone of shell side	$\Delta p = 0.334f_{eff}C_iC_n\frac{nG^2}{2\rho},$ $C_i = (cos\beta)^{-1.8}(cos\phi)^{1.355}$ $C_n = 1 + \frac{0.375}{n}$ $\beta = \alpha\left(1 - \frac{\alpha}{90}\right)$ $\phi = \alpha + \beta$	Gilli
Single-phase liquid zone	$f = \begin{cases} f_s\frac{21.5D_H}{\{1.56 + \log_{10} D_H\}^{5.73}}, 13.5 < Re < Re_c \\ \left[0.029 + 0.304\left\{Re\left(\frac{d_i}{D_c}\right)^2\right\}^{-0.25}\right]\left(\frac{d_i}{D_c}\right)^{0.5}, Re > \end{cases}$	Ito
Two-phase liquid zone	$\left(\frac{dp}{dz}\right) = \varphi_l^2\left(\frac{dp}{dz}\right)_l,$ $\varphi_l^2 = 0.0986\varphi_{LM}^2\left[Re_l\left(\frac{d_i}{D_c}\right)^{0.5}\right]^{0.19}\left(\frac{\rho_m}{\rho_l}\right)^{-0.40},$ $\varphi_{LM}^2 = \left(1 + \frac{C}{\chi_{tt}} + \frac{1}{\chi_{tt}^2}\right)$	Colombo

Chen and Miropol'skiy are more widely used correlations, but they are modeled for straight horizontal tubes. Unlike horizontal tubes, helical tubes experience centrifugal force. During the two-phase flow, liquid with higher density moves away from the center of the curvature due to larger centrifugal force. If the ratio of tube diameter to helical diameter is small, then helical tube can essentially be seen as a horizontal tube, but HTR-PM's ratio is 0.08. Thus, Yang and Xiao's revised versions were used, as they were modeled for helical tubes.

2.3 Computational Model Description

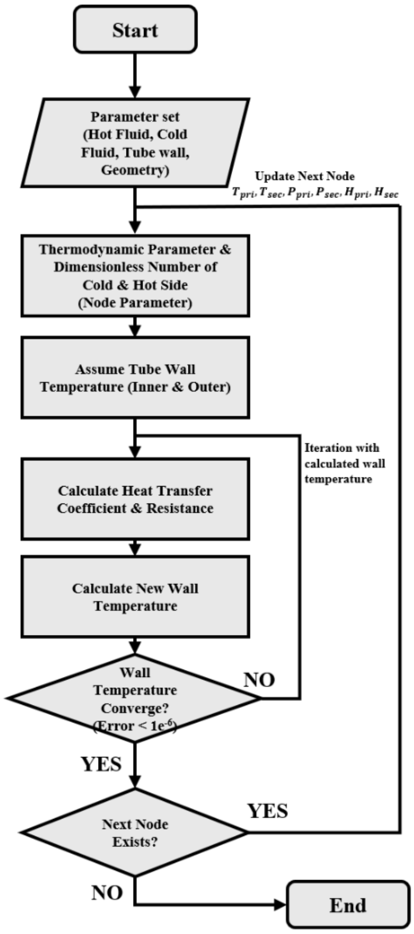

Figure 2: Logic flow chart of computational model

The model in Fig. 2 explains how the code was designed in MATLAB. First, all input parameters are defined. The tube is split into 200 nodes in the axial direction. Thermodynamic properties at the first node are calculated using these parameters, and wall temperature (T_{wall}) is estimated as the average temperature of both coolants. Then, using the properties, heat transfer from primary coolant to outer wall, outer wall to inner wall, and inner wall to secondary side are computed. If the calculated secondary coolant's temperature deviates from the prescribed temperature (initial boundary condition), the estimated value is adjusted, and the code iterates. Once the iteration is complete, the next node is updated, and the code iterates again for that node. The process is repeated for subsequent nodes until the entire tube length is analyzed.

3. Results and Discussions

The constructed numerical model with given parameters is shown in Fig. 3. The optimal tube length is determined to be 24.2 m when the temperature of primary and secondary coolants reach the given boundary condition. The temperature rises steadily up to 14 m in a single-phase liquid flow (x<0) region. Then, water starts boiling, and the temperature of water stays constant during phase transition. At 19 m, the tube wall experiences a sharp rise in temperature when the flow reaches the liquid deficiency zone; at this zone, most of the thin liquid film from annular flow evaporates. Since the heat transfer coefficient of vapor is significantly lower than that of liquid, the temperature rises abruptly. When the liquid evaporates completely and the flow turns into a single-phase flow of vapor, the temperature rises again up to the designed outlet temperature.

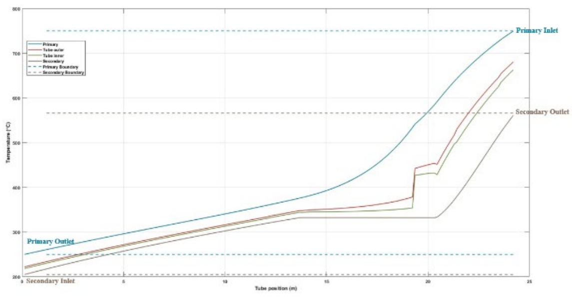

Figure 3: Temperature variation of primary coolant, tube wall, and secondary coolant along the tube length

Two correlations were newly tested for the saturated boiling and liquid deficiency zone to improve the design process. These correlations are shown in Tables IV and V. Since the temperature and pressure at which water enters different flowing regime does not change, correlation of a regime can be singly replaced to examine the effect of new correlation at the regime.

Table IV: Correlations for calculating heat transfer coefficient at saturated boiling zone for helical tubes

Researchers	Correlations
Guo	$\frac{h_{tpc}}{h_{lc}} = 7.51\left(\frac{1}{X_{tt}}\right)^{0.727}\left(\frac{p}{p_c}\right)^{0.577}$ $\frac{h_{lc}d}{\lambda_l} = 0.021Re_l^{0.8}Pr_l^{0.4}\left(\frac{d}{D}\right)^{0.1}$, $Re_l = \frac{Gd}{\mu_l}$
Zhao	$h_{TP} = Fh_l$, $F = 1.6(X_{tt})^{-0.74} + 183{,}000Bo^{1.46}$ $h_l = \frac{1}{41}Re_l^{0.8}Pr_l^{0.4}\left(Re_l\left(\frac{d}{D}\right)^2\right)^{1/20}\frac{k_l}{d}$

Table V: Correlations for calculating heat transfer coefficient at liquid deficiency zone for helical tubes

Researchers	Correlations
Guo	$\frac{h_{tpc}}{h_{lc}} = 26.5\left(\frac{1}{X_{tt}}\right)^{-0.248}$
Xiao	$Nu_g = 0.00567\left[\frac{GD}{\mu_g}\left(x + \frac{\rho_g}{\rho_l}(1-x)\right)\right]^{0.565} Pr_g^{-0.245}Y$, $Y = \left[1 - 0.1\left(\frac{\rho_l - \rho_g}{\rho_g}\right)^{0.4}(1-x)^{0.4}\right]^{-4.5}\left(\frac{4q}{h_{fg}G}\right)^{-1.1}\left(\frac{1}{X_{tt}}\right)^{-0.447}$

Tables IV and V show correlations that are tested for helical tubes [4]. Correlations were implemented individually, while keeping other correlations the same, to see change in each zone after changing the correlations.

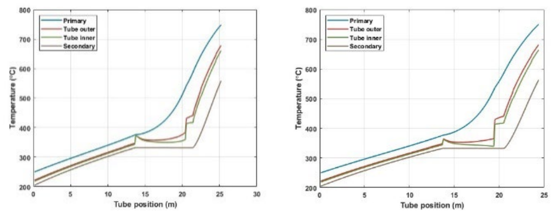

Figure 4: Temperature variation using (a) Zhao and (b) Guo's correlation along the tube length

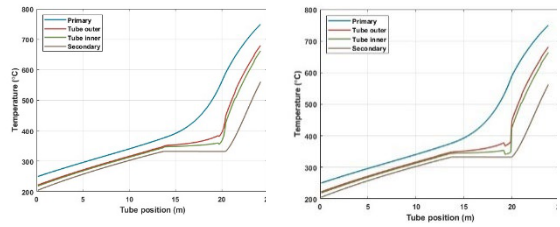

Figure 5: Temperatures at varying tube positions using (a) Xiao and (b) Guo's correlation

Fig. 4 displays implementation of Zhao and Guo correlations instead of Yang. The optimal tube length for Zhao correlation is 25.2 m, and Guo suggests 24.4 m. The Zhao correlation in Fig. 4a exhibits a sudden increase in wall temperature at the onset of boiling. This means that the prediction of the heat transfer coefficient using Zhao is much higher than that of Hardik, which makes a sharp rise in temperature at that node. However, a jump seems non-physical, meaning Zhao correlation overpredicts the heat transfer coefficient. Guo's correlation also shows a jump in Fig. 4b. Moreover, both correlations show that the wall temperature decreases. Zhao's correlation increases back at a point while Guo's decreases until the flow reaches liquid deficiency zone. This shows that Yang's modification of Chen's correlation can produce the most physically acceptable results for the two-phase heat transfer in a helical tube.

Fig. 5 displays Xiao and Guo correlations replacing Xu correlation. The optimal tube length for Xiao is 24.2 m, and the optimal tube length for Guo is 23.8 m. In Fig. 5b, temperature stays relatively constant after jumping until the flow turns into a single-phase flow. In Fig. 5a, there is no jump, but the wall temperature increases steeply until the flow becomes single-phase flow. Fig. 65 shows reversed behavior from Fig. 3 as the temperature slowly decreases initially in the liquid deficiency zone, and the wall temperature experiences a jump at the end of the zone, just before entering the single-phase flow zone. Also, Guo's correlation predicts that the temperature jump is bigger than Miropol'skiy's, which is why the optimal length calculated is 0.4 m shorter. Xiao correlation is likely the better prediction of heat transfer, as previous studies claim that the jump in T_{wall} is roughly 30-50℃ [2]. Also, a jump is more likely to happen at the beginning of the liquid deficiency zone, not at the end.

4. Conclusions and Further Works

This study developed a numerical model to simulate heat transfer in the helical steam generator of HTR-PM using different correlations. The model incorporated the iteration method after splitting tubes into nodes to see the change in flow regimes inside the steam generator at different tube positions. Different correlations were used at the two-phase flow and liquid deficiency zone to see differences between the correlations. The optimal combination of correlations is shown in Table VI below. This combination shows the most physically acceptable model.

Table VI: Optimal correlation combination for HTR-PM

Zone	Correlation
Single-phase liquid zone (shell side)	Žukauskas
Single-phase liquid zone (tube side)	Schmidt
Subcooled boiling zone	Hardik
Saturated boiling and forced convection evaporation zone	Yang
Liquid deficiency zone	Xiao
Single-phase vapor zone	Mori & Nakayama

There are clear limitations to this analysis. First, not all parameters are the operating parameters of HTR-PM, as they are not disclosed to the public, and they had to be approximated. Second, the geometry has been simplified to a single tube analysis, where tube's diameter was assumed as averaged value of geometric parameters. However, tube geometries vary depending on the layer. Third, the HTR-PM's parameters are beyond the suggested parameters of the correlations used.

As for the direction of subsequent research, actual experiments can be conducted to validate the model with experimental data. Also, there is a possibility that all parameters and running data of HTR-PM will be disclosed at one point in the future, which can be used for validation of the model. The sensitivity analysis of various parameters will be conducted to find the optimal geometry.

ACKNOWLEDGEMENT

This work was supported by the Innovative Small Modular Reactor Development Agency grant funded by the Korea Government (MOTIE) (No. RS-2024-00404240).

REFERENCES

[1] Wu, Z., Lin, D., & Zhong, D. (2002). The design features of the HTR-10. Nuclear Engineering and Design, 218(1–3), 25–32.

[2] Sun, J., Zhang, R., Wang, M., Zhang, J., Qiu, S., Tian, W., & Su, G. H. (2022). Multi-objective optimization of helical coil steam generator in high temperature gas reactors with genetic algorithm and response surface method. Energy, 259, 124976.

[3] ZHANG, Z., YANG, X., & JU, H. (2015). ICONE23-1474 design and thermal-hydraulic analysis of supercritical steam generator in high-temperature gas-cooled reactor. The Proceedings of the International Conference on Nuclear Engineering (ICONE), 2015.23(0).

[4] Gou, J., Ma, H., Yang, Z., & Shan, J. (2017). An assessment of heat transfer models of water flow in helically coiled tubes based on selected experimental datasets. Annals of Nuclear Energy, 110, 648–667.